**Proceedings of FEDSM'99**
**3rd ASME/JSME Joint Fluids Engineering Conference**
**July 18-23, 1999, San Francisco, California, USA**

**FEDSM99-6934**

# TURBULENCE MODULATION BY AN ARRAY OF LARGE-SCALE STREAMWISE STRUCTURES OF EHD ORIGIN

**Marco Fulgosi and Alfredo Soldati***

Centro Interdipartimentale di Fluidodinamica e Idraulica
Dipartimento di Scienze e Tecnologie Chimiche
Università degli Studi di Udine
Udine, 33100, Italy
Email: alfredo@euterpe.dstc.uniud.it

**Sanjoy Banerjee**

Department of Chemical Engineering
University of California at Santa Barbara
Santa Barbara, California, 93106
Email: banerjee@anemone.ucsb.edu

## ABSTRACT

Recently, it was shown (Schoppa and Hussain, *Phys. Fluids*, **10**, 1049) that superimposing large-scale, *synthetic*, streamwise vortical flow structures onto a turbulent Poiseuille flow led to suppression of the low-speed streak instability mechanism, which, in the end, appears to be responsible for drag enhancement in turbulent flows. In this work, we use large-scale ElectroHydroDynamic flow structures to control turbulent transfer mechanisms. We consider a channel with two different flow control configurations: E-control, in which streamwise wire-electrodes are embedded into one of the walls and C-control, in which streamwise wire-electrodes are placed in the central-plane of the channel. In all cases, the wires are maintained at a potential sufficient to ensure ionic discharge. Ions are driven by the applied electrostatic field and generate plane, streamwise jets, which impinge on the opposite (grounded) wall and, by continuity, generate two-dimensional vortical flows. Control flows have a spanwise periodicity of 340 wall units, in order to encompass three low-speed streaky structures.

Results indicate that, after flow control actuation, the flow field undergoes an initial steep transient of about 600 shear-based time units with a moderate drag decrease (about $6-7\%$), followed by a steady-state in which the overall drag is only slightly modified. All cases with E-control indicated drag increase. Higher intensity C-control cases led to drag reduction. The long-term effect of flow control is small, being at most about $4-5\%$. Corresponding to such small modification of the overall drag there is no significant change in the structure of turbulence at the wall.

## INTRODUCTION

Chances of decreasing drag in aeronautical and marine vehicles, and of increasing the efficiency of combustion devices prompted research work in turbulence control. The key for turbulence control is controlling turbulent transfer mechanisms which, in turn, are dominated by Coherent Structures. For example, in a turbulent boundary layer, streamwise coherent structures have been linked to bursts and sweeps, which take slow-moving wall fluid into the outer region and bring fast-moving outer fluid into the wall region. These events generate a major portion of the drag and are well correlated with heat and mass transfer fluxes.

In recent times, research has been focused on active control strategies, which are based, first, on the detection of the events producing drag and, second, on generating local fluid motions able to counteract the drag producing events (see, among others, Jacobson and Reynolds, 1998). Since the scale of these events decreases with the Reynolds number, in order to control turbulence with such techniques, a large number of sensors and actuators must be employed for usual applications.

If suitable large-scale structures could be generated economically and optimized to reduce drag, advantages could be found

*Corresponding author. Ph. ++39 0432 558864; Fax: ++39 0432 558803.

compared to the usual active control techniques. The baseline of turbulence control by large-scale structures is the possibility of controlling turbulent transfer mechanisms – drag producing mechanisms – over a large portion of the domain boundary, *i.e.* spanning over several low-speed streaks. Thus, in the first place, complex control devices are not needed. Second, since the scales of the imposed flows are much larger than the scale of the streamwise structures, the method can be used over a large range of Reynolds numbers without adjustments.

In a recent communicatione (Schoppa and Hussein, 1998) it was shown that superposition of large-scale, streamwise-independent vortical flow structures, with a spanwise wavelength of about 400 wall units, onto a turbulent Poiseuille flow, led to suppression of the low-speed streaks instability mechanism, which is thought to be responsible for regenerating the streamwise coherent structures. However, even though Schoppa and Hussein (1998) could show drag reduction, in some cases up to 50 %, their analysis was somewhat preliminary, since they did not generate the control flows by means of a physical mechanism. Rather, they superimposed *synthetic* control flows onto the turbulent field. They adopted two strategies: *i*) not to let the control flows evolve together with the turbulent field, which they named *frozen* control; *ii*) to let the control flows evolve with the turbulent field, which they named *free* control. In the case of frozen control, they could show up to 50 % drag reduction. In the free flow control cases, they could show drag reduction only for a limited transient of around 1000 time wall units.

This paper is focused on the study of physical feasibility of such control strategy. We tried to simulate physical control flows with some of the characteristics suggested by Schoppa and Hussain (1998), and examined their effect on a closed Poiseuille channel flow. Following our previous work (Soldati and Banerjee, 1998), we used electrostatic forces to generate the large-scale structures imposed on the turbulent through-flow. We considered two types of control flows: *i*) two-dimensional jets issuing from one wall and impinging on the other, aligned in the streamwise direction (*E-control*); *ii*) two-dimensional jets issuing from the center of the channel, also aligned in the streamwise direction (*C-control*). A schematic of the two configurations is given in Figure 1. The control flows do not produce a net flow throughput, but modify turbulent transfer mechanisms at the wall, which are responsible for drag production.

We used a pseudo-spectral method to solve the Navier-Stokes equations including the Coulomb body force, which was calculated using a finite-difference scheme. The body force distribution is steady and uncoupled to the flow field, since ionic drift in gases is much larger than the fluid convection velocity.

## NUMERICAL SIMULATION

The turbulent flow of air, assumed to be incompressible, Newtonian, with no-slip conditions at walls, and driven by a pressure gradient was numerically simulated for an imposed pressure gradient. The wire-electrodes necessary to generate the electrostatic body force to drive the control flows were kept at a potential sufficient to ensure ionic discharge and the presence of distributed ionic species in the duct. Ions are subjected to the Coulomb force, **F**, which may be expressed as:

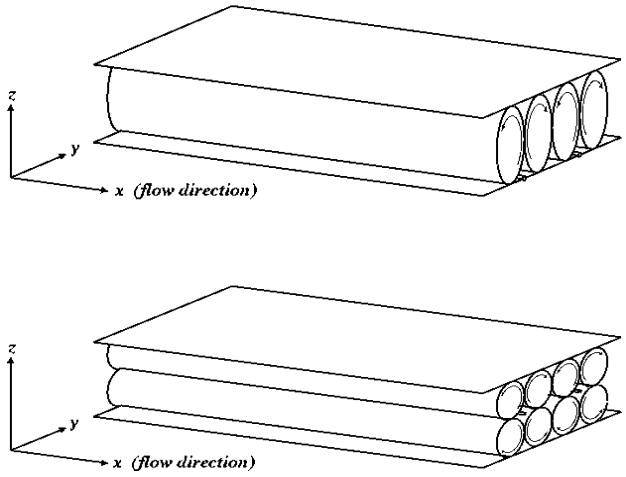


Figure 1. Schematic of control flows: a) E control: streamwise vortical structures generated by wires embedded in one wall; b) C control: streamwise vortical structures generated by wires in the middle of channel.

$$\mathbf{F} = \rho_c \mathbf{E} \quad , \tag{1}$$

where $\rho_c$ is the charge density and **E** is the electric field vector. Ions are driven toward the walls and collide with fluid molecules, transferring momentum to them. This is equivalent to a body force which acts directly on the fluid. Therefore, the equation of fluid motion in dimensional terms is

$$\rho \left[ \frac{\partial u_i}{\partial t} + u_j \frac{\partial u_i}{\partial x_j} \right] = -\frac{\partial P}{\partial x_i} + \mu \frac{\partial^2 u_i}{\partial x_j \partial x_j} + F_i \quad , \tag{2}$$

where $u_i$ are the dimensional velocity components along the three directions $x_i$ (with $x_1$, or $x$ being streamwise, $x_2$ or $y$ being spanwise and $x_3$ or $z$ being the wall-normal directions), $P$ is pressure, and $\rho$ and $\mu$ are fluid density and dynamic viscosity, respectively. For the case under consideration, the body force depends only on $y$ and $z$, implying that the body force distribution does not fluctuate because of ionic convection. This is a realistic assumption, since ions have a drift velocity of about a hundred meters per second in air while the mean flow velocity is about one meter per second. For liquids, ionic convection may not be negligible

in some situations and "two-way" coupling will exist between the flow field and the electrostatic body force field. Here the coupling is "one-way", *i.e.* the flow field does not modify the electrostatic body forces.

### Flow Field

The flow field was calculated by integrating mass and momentum balance equations in dimensionless form obtained using the duct half-width, $h$, and the shear velocity, $u_\tau$, defined as

$$u_\tau = \sqrt{\frac{\tau_w}{\rho}} \tag{3}$$

where $\tau_w$ is the shear at the wall. Therefore, mass and momentum balance equations in dimensionless form are

$$\frac{\partial u_i}{\partial x_i} = 0 \quad , \tag{4}$$

and

$$\frac{\partial u_i}{\partial t} = -u_j \frac{\partial u_i}{\partial x_j} + \frac{1}{Re} \frac{\partial^2 u_i}{\partial x_j \partial x_j} - \frac{\partial p}{\partial x_i} + \delta_{1,i} + \Phi_i \quad , \tag{5}$$

where $u_i$ is the $i$th component of the dimensionless velocity vector, $\delta_{1,i}$ is the mean dimensionless pressure gradient, $\Phi$ is the dimensionless electrostatic body force, and $Re_\tau = hu_\tau/\nu$ is the shear Reynolds number. Eqs. 4 and 5 were solved directly using a pseudo-spectral method similar to that used by Kim *et al.* (1987) to solve the turbulent, closed-channel flow problem. The difference is the inclusion of the space dependent body force which, being steady and uncoupled to the flow field, was calculated once at the beginning of each simulation. If the body force term is treated together with the non-linear terms, Eq. 5 may be recast as:

$$\frac{\partial u_i}{\partial t} = S_i + \frac{1}{Re_\tau} \frac{\partial^2 u_i}{\partial x_j \partial x_j} - \frac{\partial p}{\partial x_i} \tag{6}$$

which is identical to forms previously solved (Kim *et al.* , 1987, Lam and Banerjee, 1992), and where $S_i$ now includes the convective term, the mean pressure gradient and the Coulomb term. The pseudo-spectral method is based on transforming the field variables into wave-number space, using Fourier representations for the streamwise and spanwise directions and a Chebyshev representation for the wall-normal (nonhomogeneous) direction. A two level, explicit, Adams-Bashforth scheme for the non linear terms $S_i$ and an implicit Crank-Nicolson method for the viscous terms were employed for time advancement. Details of the method have been published previously (Lam and Banerjee, 1992).

Considering air with density of $1.38\ kg/m^3$, and kinematic viscosity of $16.6 \cdot 10^{-6}\ m^2/s$, since the pressure gradient is imposed equal for all simulations, the shear velocity is $8.964 \cdot 10^{-2}\ m/s$, and the shear Reynolds number is equal to 108. For the reference case with no EHD effects (Soldati *et al.* , 1993), the mean velocity is $1.16\ m/s$ and the Reynolds number based on mean velocity and duct width is $\sim 2795$. The grid is $64 \times 64 \times 65$ in the streamwise, spanwise and wall normal directions respectively, which gives a resolution comparable to that of other well known DNS databases (Kim *et al.* , 1987, Lyons *et al.* , 1991, Lam and Banerjee, 1992) for this Reynolds number.

### Body Force Control Field

The electrostatic potential distribution and space charge distribution are given by the following set of equations:

$$\frac{\partial^2 V}{\partial x_i^2} = -\frac{\rho_c}{\varepsilon_0} \tag{7}$$

$$\rho_c^2 = \varepsilon_0 \frac{\partial \rho_c}{\partial x_i} \frac{\partial V}{\partial x_i} = -\varepsilon_0 \frac{\partial \rho_c}{\partial x_i} E_i \tag{8}$$

$$E_i = -\frac{\partial V}{\partial x_i} \tag{9}$$

$$J_i = -\rho_c \beta E_i \quad . \tag{10}$$

where, $\varepsilon_0$ is air permittivity ($\varepsilon_0 = 8.854 \cdot 10^{-12}$), and $\beta = 1.4311 \cdot 10^{-4} m^2/V\ s$ is ionic mobility (McDaniel and Mason, 1973) for positive discharge in air. Eqs. 7-10 were solved by a two dimensional finite difference scheme (Leutert and Bohlen, 1972, Yamamoto and Velkoff, 1981) based on an initial guess for the space charge density at the wire followed by iterative solution of Eqs. 7 and 8 until convergence of the plate current density was obtained. Details on the numerical procedure and on the validation of the body force calculation against previous numerical and experimental analyses may be found in previous works (Kallio and Stock, 1992, Fulgosi, 1998).

### Simulation of Control Flows

All simulations were started from the uncontrolled channel flow simulation calculated for a shear Reynolds number, $Re_\tau = 108$ over a grid of $64 \times 64 \times 65$ (Soldati *et al.* , 1993). The body

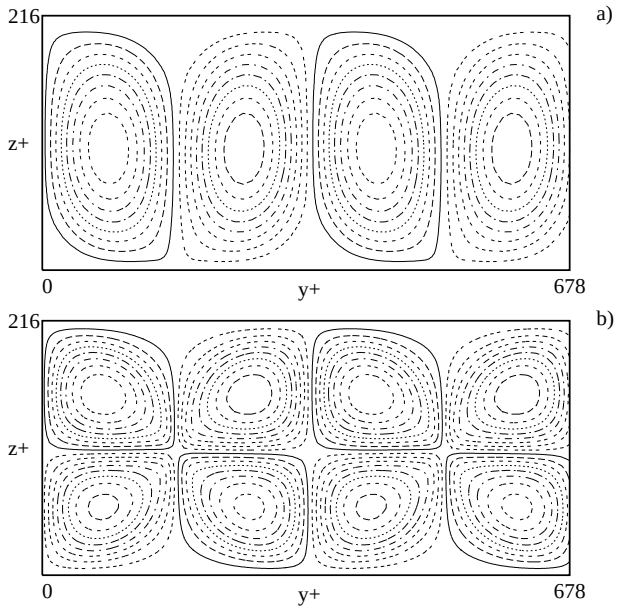


Figure 2. Streamlines of control flows for no-through flow case: a) E-control, with streamwise wires embedded in the wall; contours go from -130 to 130 with increments of 15 in wall units; b) C-control, with streamwise wires in the middle of the channel; contours go from -35 to 35 with increments of 4 in wall units.

force was applied and simulations were run until a new steady state was reached. The wires were kept at a potential of 15 000 $V$ for all simulations while the current flowing through the duct was varied. This allowed to have control flows of different intensity. After the steady state was reached, simulations were continued for a number of time steps sufficient to obtain adequate statistics.

The control variable in this type of flow control is the intensity of the electric current flowing through the duct. However, this information is not directly related to the structure of the turbulence field, and the organized control-flow flowrate should be used (Schoppa and Hussein, 1998). It is not straightforward to predict a-priori the intensity and the shape of the control flows once they have been interacting with the turbulent through-flow. We characterized the control flows on the basis of the shape and intensity they assumed in a no-through flow case. Since in this case there is no applied pressure gradient and, consequently, there is no net flow through the duct, we calculated the flowrate of each convective EHD cell. In Figure 2 a) and b), the streamlines of the flow field obtained for a zero pressure gradient are shown for one of the E cases and one of the C cases respectively. In all cases, the wire-electrodes had a spanwise spacing of 340 wall units. The flow structures are two-dimensional and reflect the distribution of the body force. Current intensity and the corresponding flowrates for the six cases investigated are reported in Table 1. The flowrates are normalized by the flowrate of the channel with no imposed flow.

Table 1. SUMMARY OF THE SIMULATIONS

| | Current Density $(A/m^2)$ | $W_{control}/W_{channel}$ (%) |
|---|---|---|
| **E1** | 1.50E-05 | 12.7 |
| **E2** | 2.00E-05 | 17.4 |
| **E3** | 5.00E-05 | 48.5 |
| **C1** | 1.00E-07 | 2.7 |
| **C2** | 5.00E-06 | 8.3 |
| **C3** | 2.00E-05 | 25.2 |

## RESULTS

### Overall Drag Modification

Since the pressure drop is the same for all the simulations, drag changes are indicated by the behavior of the streamwise mean velocity. The behavior of the mean streamwise velocity versus time is presented for the E-control flow case, in Figure 3 a), and for the C-control flow case, in Figure 3 b).

After flow control actuation, there is a transient lasting about 600 dimensionless time units in which the mean velocity increases for all the simulations. At present, there is no clear understanding of the reasons leading to such transient behavior. Considering the E-control flow cases, all simulations attain a steady state in which the velocity is lower than the corresponding uncontrolled flow case. Variations are, in any case, modest, with a maximum decrease of about 3% in case E3, in which the control flows are strongest. Drag behavior with the intensity of the EHD flows is monotonic, suggesting that this configuration may not be optimized for drag reduction. The application of C-control flows gives a more complex behavior of the overall drag with the intensity of the control flows: at very low intensity, drag is increased, whereas for higher intensity drag is increasingly reduced. In cases C2 and C3 the mean velocity reaches a steady state with increases of 2% and 3% respectively. While the effect on drag of the imposed flows is small, being at most of the order of 4 – 5%, no attempt has been made to optimize the various parameters.

### Identification of Control Flows

To identify a strategy to optimize the shape and intensity of control flows, a proper characterization of the control flow itself is necessary. Considering that the actuating body force is two-dimensional and steady, a suitable filtering of the flow field should allow characterization of the control flows. One possibility is averaging over the streamwise direction for an adequate length, which could be, for instance, the length of the computational box – also scaling with the length of low-speed streaks – and is based on the hypothesis that the flow field is given as the

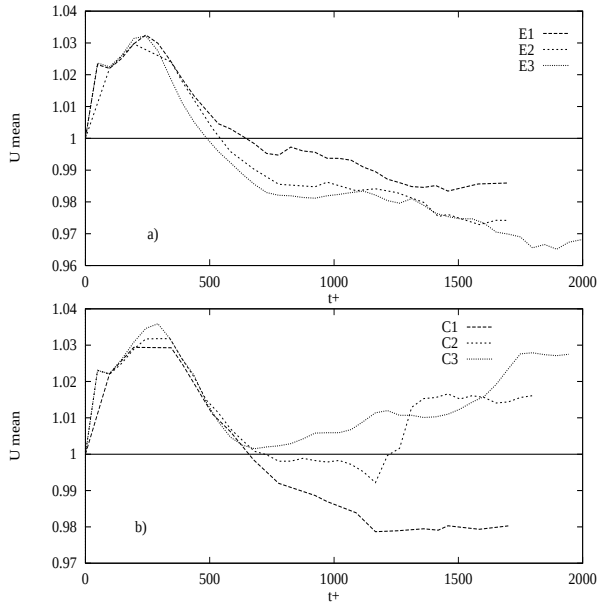


Figure 3. Evolution of mean through velocity with time for a) E-control, and b) C-control for all simulated cases, normalized with mean-through velocity of unforced channel flow case. After increase, mean velocity reaches steady state for all simulations. In all E-control cases, mean velocity is lower than corresponding unforced flow case. In C-control, increase of mean velocity is obtained for higher body force intensity.

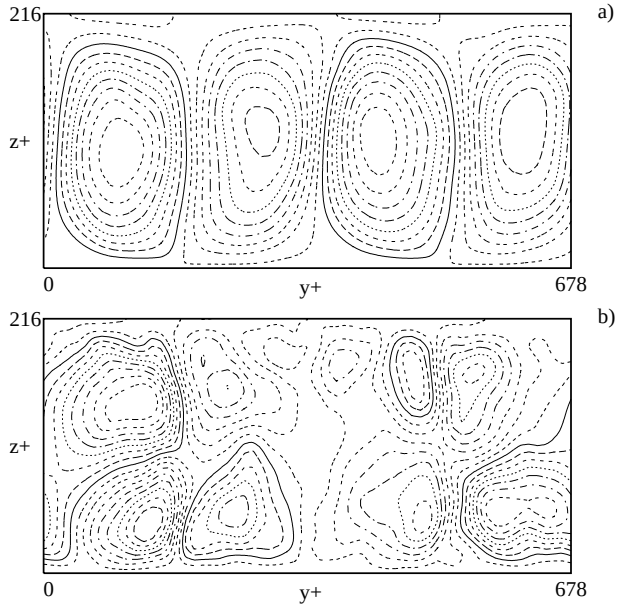


Figure 4. Filtered streamlines of control flows for highest potential applied for a) E-control, with contours going from -90 to 90 with increments of 11.25 in wall units; and b) C-control, with contours going from -28 to 20 with increments of 3 in wall units: average value of maximum streamline was obtained averaging over the different vortical flows.

superposition of a mean velocity field, $\overline{u}$, driven by the pressure gradient, a turbulence field, $u'$, and the organized control flow field, $\tilde{u}$, driven by the electrostatic body force. This triple decomposition was applied successfully in our previous paper (Soldati and Banerjee, 1998) to identify large-scale spanwise organized flows.

In Figure 4 a), the isocontours of the streamlines corresponding to case E3 are shown. The streamlines have been obtained averaging the flow field in the streamwise direction and subtracting the mean streamwise velocity. The streamlines show a weak modification in their shape if compared to those presented in Figure 2 a). However, the total flowrate of the control flows is now 31.5% of the channel flowrate, indicating a large reduction with respect to the no-through flow case (48.5%). The streamlines corresponding to case C3 are shown in Figure 4 b). In this case, the control flows appear to be significantly perturbed by the turbulent through flow. The total flowrate of the control flows is now 17.6% of the channel flowrate, and this value was obtained averaging the maxima of the single vortical structures.

A similar procedure was applied to the other cases at lower intensity of the control flows, trying also to increase the length over which the average was carried out over the whole database, but no clear pattern was identified which could be traced back to the pattern that the control flow has in the no-through flow case. This can be explained considering that all turbulence structures in a boundary layer are aligned in the streamwise direction. The interaction and superposition of these structures with the streamwise control flows made difficult a clear identification of the control flows and, consequently, the determination of their flowrate using this triple decomposition.

## Mean Velocity and Turbulence Intensity

The profiles of the mean velocity for the uncontrolled channel flow case is compared against the mean velocity profile of the E-control cases in Figure 5 a) and of the C-control cases in Figure 5 b). In the E-control cases the wires are located at $z^+ = 0$. Considering first Figure 5 a), all profiles are flattened in the center of the channel. Also in the C-control cases the profiles appear flattened in the center of the channel, but they increase in the wall region, producing, in the two cases at higher potential, a net increment in the flow throughput.

Modification of turbulence intensity is shown in Figure 6. As observed in the previous section, the flow field may be considered as given by the superposition of the mean field, the turbulence field and the organized control flow field. The evaluation of turbulence intensity should be made only on the turbulence field, thus filtering out mean flow and control flow components (Soldati and Banerjee, 1998). At this stage, a suitable filtering procedure was not identified and applied. However, since the control flows are streamwise independent, they give no direct contribu-

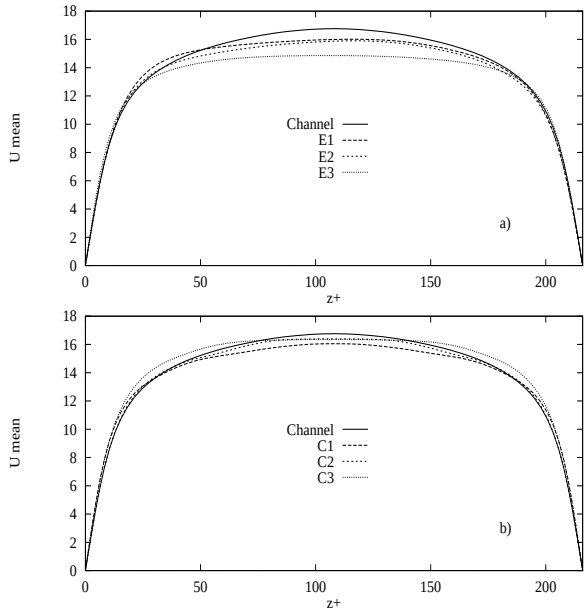


Figure 5. Behavior of mean velocity profile for a) E-control, and b) C-control for all simulated cases, compared with velocity profile of unforced channel flow case. In all cases, profile is flattened in channel center.

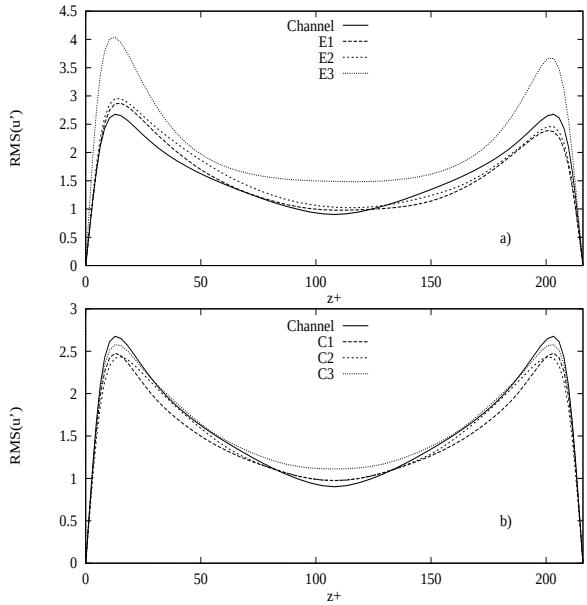


Figure 6. Variance of velocity fluctuations in the streamwise direction for a) E-control cases, and b) C-control cases, compared with turbulence intensity of the uncontrolled channel flow case.

tion to turbulence intensity in the streamwise direction.

The intensity of turbulence in the streamwise direction is shown in Figure 6 a) for E-control cases. Turbulence intensity is increased close to the wall from which the jets issue, *i.e.* the one with the embedded wires, and decreased close to the other wall for all cases with the exception of case E3, in which large turbulence intensity is observed throughout the channel. In all cases, however, the increase of the intensity of control flows produces a monotonic trend in the modification of turbulence intensity.

In Figure 6 b), the intensity of turbulence in the streamwise direction is shown for the C-control cases. In all C-control cases, turbulence intensity decreases in the wall region and increases in the central region of the channel. Compared to the uncontrolled channel flow case, for increasing intensity of the control flows there is an initial decrease of turbulence intensity in the wall region – cases C1 and C2 – followed by an increase of turbulence intensity in case C3. This indicates that after initially damping turbulence production mechanisms, higher intensity control flows increase turbulence level producing turbulence by their own mechanisms (Soldati and Banerjee, 1998).

### Instantaneous Structure of Turbulence under C-control

In this section, we will consider the structure of turbulence in the wall region for the C-control cases, because this configuration seems more promising from the point of view of drag reduction.

The streaky structure of the fluctuating streamwise velocity component is one fingerprint of turbulent boundary layers. In Figure 7 a), the streaky structures of the uncontrolled channel flow cases are shown. It is well known that streaky structures are linked to regions of high and low shear stress at the wall: a low speed streak is a region of low shear stress, whereas a high speed patch is a region of high shear stress. This link can be appreciated comparing Figure 7 b), where the instantaneous distribution of the wall shear stress is mapped, with Figure 7 a). A region of low streamwise fluctuating velocity indicates an uplift of wall fluid toward higher speed layers – burst. This causes a local decrease of the wall shear stress. A region of high streamwise fluctuating velocity indicates a downdraft of higher momentum fluid toward the wall – a sweep – which causes an increase in the local wall shear stress. Ultimately, the dynamics of the streaks is related to the dynamics of the coherent structures which control momentum transfer in the boundary layer. As observed by Schoppa and Hussain (Schoppa and Hussein, 1998), large modification of the skin friction are related to the disruption of such coherent structures. On the other hand, as already put in evidence in other works (*e.g.* , Lombardi *et al.* , 1996, Soldati and Banerjee, 1998), small modifications of the wall shear stress, and hence of the total drag, can be found also in cases in which the dynamics of the coherent structures of the boundary layer retains its characteristics, but intensity and frequency of single events, *e.g.* sweeps and bursts, are somewhat modified. In Figures 8 – 10, the streaky structure and the wall shear stress distribution for the C-control cases are shown. The effect of control jets can be observed only in case C3, Figure 10, where two streaks appear more pronounced.

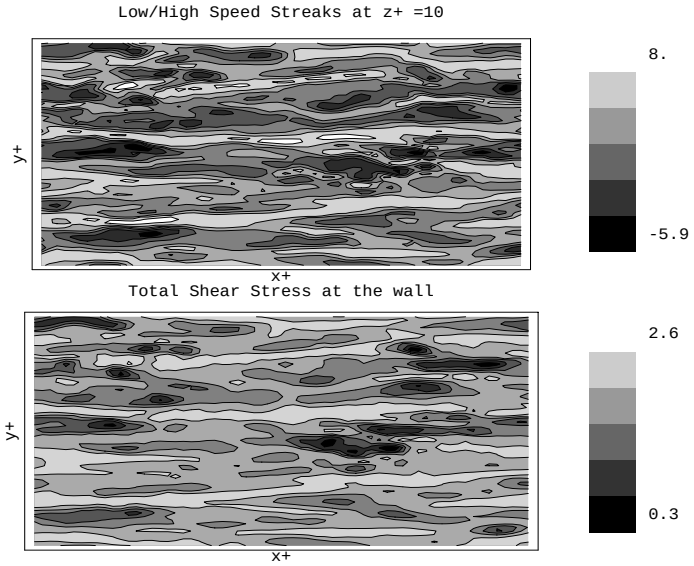


Figure 7. Streaky structures in the boundary layer at $z^+ = 10$ a); and instantaneous wall shear distribution in the uncontrolled flow case b).

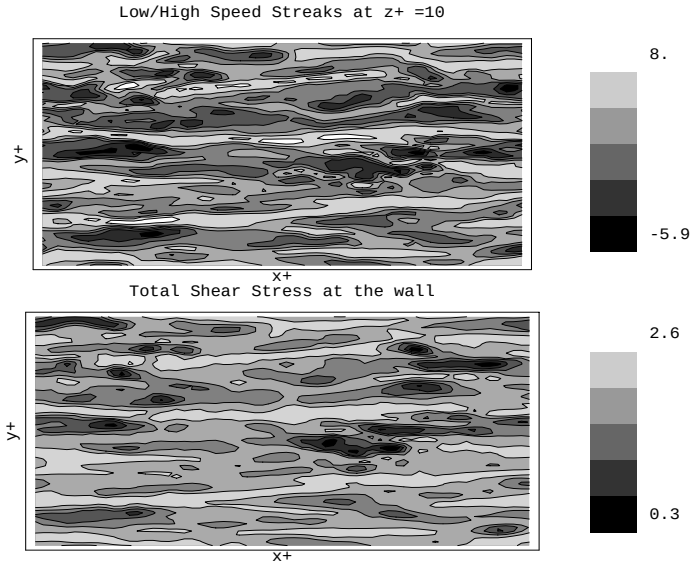


Figure 8. Streaky structures in the boundary layer at $z^+ = 10$ a); and instantaneous wall shear distribution in C1 control flow case b).

An examination of the streak spacing for a number of different timesteps gave results altogether similar to those obtained for the uncontrolled channel flow, indicating that the structure of the boundary layer is not markedly affected by the presence of the control flows.

## CONCLUSIONS AND FUTURE DEVELOPMENTS

In this work, we tried to examine physical realization of the situation approximating the suggestion of Schoppa and Hussain (1998) who demonstrated that superimposing synthetic control flows in the shape of large-scale streamwise structures, which could encompass several low-speed streaks, can significantly reduce drag in a turbulent boundary layer. This technique appears interesting from a practical viewpoint since actuation of control flows does not require the accurate knowledge of turbulence structure at the wall. We used control flows of electrohydrodynamic origin generated by the flow of ionic species discharged from streamwise wires placed in different configurations. As shown by Roth *et al.* (1998), EHD can be the preferred approach for flow control compared to the more investigated Magneto-HydroDynamic approach (Tsinober, 1989). We considered two flow control configurations: E-control, with wires embedded into one wall, leading to EHD jets that generate 2D vortical flows of the scale of the wall-to-wall distance, and C-control, with wires placed in the middle of the channel, leading to jets generating 2D vortical flows of the scale of half the wall-to-wall distance. We performed Direct Numerical Simulations for each flow control configuration, and examined the effect of different intensity of the control flows.

Preliminary analysis of the results indicated that application of the electrostatic control produced a transient of about 600 shear-based time units during which drag was reduced by about $6-7\%$ in all cases. After the initial transient, a new steady state was reached. In all E-control cases, the mean velocity was moderately reduced (at most 3%), whereas in the higher intensity C-control cases the mean velocity was moderately increased (at most 3%). The structure of the turbulent boundary layer was examined. In particular for the C-control cases, no disruption of the streaky structure was observed. Rather, we found structures with characteristics similar to those occurring in uncontrolled channel flow. Drag modification observed in all cases is probably due to the bias induced in the balance between turbulent drag producing events and turbulent drag reducing events. Further analysis is required in order to investigate on the interaction between control flows and structures in the turbulent boundary layer. This is necessary before proceeding toward an optimization of shape and intensity of the control flows.

At present, we are examining different control flow configurations which should be more effective for turbulence control. We are developing a procedure to simulate wall-parallel large-scale jets in the spanwise direction. The mechanisms by which wall-jets should reduce turbulent drag are the same as on which drag-reduction by wall oscillations are based (Jung *et al.* , 1992, Choi and Graham, 1998). These techniques are based on *out-phasing* the streamwise structures in the wall region in order to affect the low-speed streak instability mechanisms, which is believed to be responsible for regenerating the streamwise coherent structures, which, in turn, appear to be the cause of drag enhancement in a turbulent boundary layer.

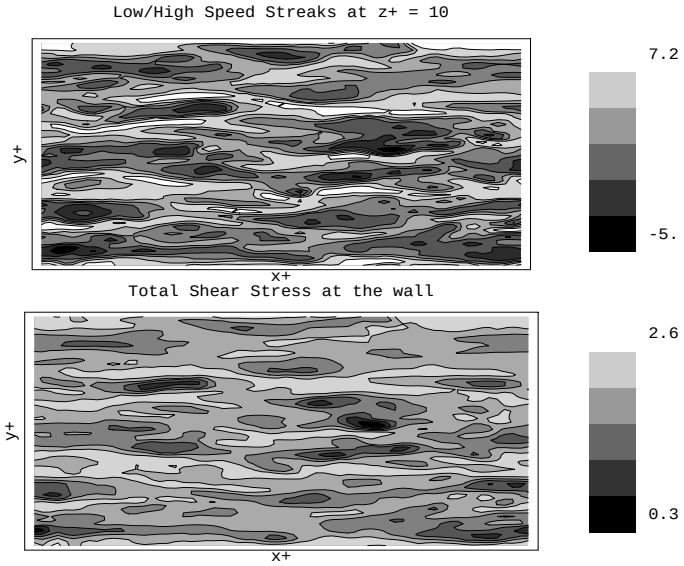


Figure 9. Streaky structures in the boundary layer at $z^+ = 10$ a); and instantaneous wall shear distribution in C2 control flow case b).

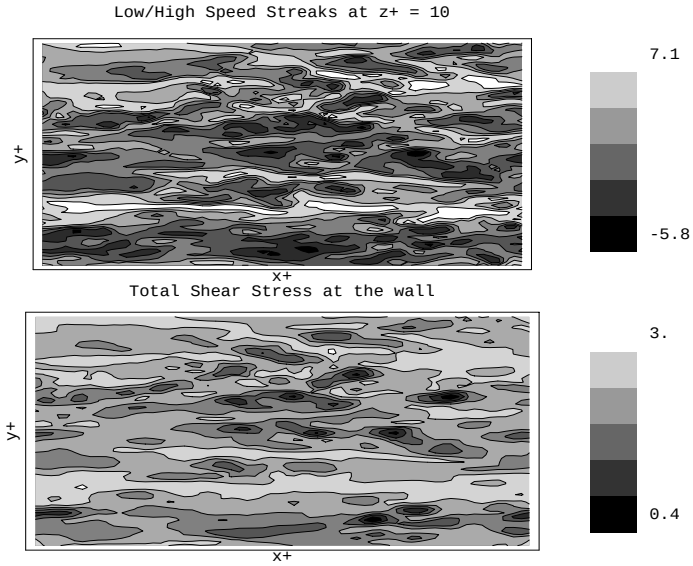


Figure 10. Streaky structures in the boundary layer at $z^+ = 10$ a); and instantaneous wall shear distribution in C3 control flow case b).


## ACKNOWLEDGMENT

Computational resources provided by ENEL/CRT, Pisa, Italy on their CRAY Y-MP2/232 are gratefully acknowledged.


## REFERENCES


S. A. Jacobson and W. C. Reynolds (1998) "Active control of streamwise vortices and streaks in boundary layers", *J. Fluid Mech.*, **360**, 179.

W. Schoppa and F. Hussain (1998) "A large-scale control strategy for drag reduction in turbulent boundary layers", *Phys. Fluids*, **10**, 1049.

A. Soldati and S. Banerjee (1998) "Turbulence modification by large scale organized electrohydrodynamic flows", *Phys. Fluids*, **10**, 1742.

J. Kim, P. Moin, and R. Moser (1987) "Turbulence statistics in fully developed channel flow at low Reynolds number," *J. Fluid Mech.* **177**, 133.

K. Lam and S. Banerjee (1992) "On the condition of streak formation in bounded flows," *Phys. Fluids A* **4**, 306.

A. Soldati, P. Andreussi, and S. Banerjee (1993) "Direct simulation of turbulent particle transport in electrostatic precipitators," *AIChE J.* **39**, 1910.

S. L. Lyons, T. J. Hanratty and J. B. McLaughlin (1991) "Large-scale computer simulation of fully developed channel flow with heat transfer," *Int. J. Num. Methods in Fluids* **13**, 999.

E. W. Mc Daniel and E. A. Mason (1973) *The mobility and diffusion of ions in gases* (Wiley, New York).

G. Leutert and B. Bohlen (1972) "The spatial trend of electric field strength and space charge density in plate type electrostatic precipitator," *Staub Reinhalt Luft* **32**, 27 (in English).

T. Yamamoto and H. R. Velkoff (1981) "Electrohydrodynamics in an electrostatic precipitator," *J. Fluid Mech.* **108**, 1.

G. A. Kallio and D. E. Stock (1992) "Interaction of electrostatic and fluid dynamic fields in wire-plate electrostatic precipitators," *J. Fluid Mech.* **240**, 133.

M. Fulgosi (1998) "Large scale control strategy for control of turbulent boundary layers," M.S. Thesis, University of Udine, Italy (In Italian).

P. Lombardi, V. De Angelis, and S. Banerjee (1996) "Direct numerical simulation of near-interface turbulence in coupled gas-liquid flow," *Phys. Fluids* **8**, 1643.

J. R. Roth, D. M. Sherman, and S. P. Wilkinson (1998) "Boundary layer flow control with a one atmosphere uniform glow discharge surface plasma," AIAA Paper No. 98-0328.

A. Tsinober (1989) "MHD flow drag reduction," *Viscous drag reduction in boundary layers* AIAA Progress in Astronautics and Aeronautics, **123**, A. R. Seabass Ed., 327.

W. Jung, N. Mangiavacchi, and R. Akhavan (1992) "Suppression of turbulence in wall-bounded flows by high frequency spanwise oscillations," *Phys. Fluids* **4**, 1605.

K-S. Choi and M. Graham (1998) "Drag reduction of turbulent pipe flows by circular-wall oscillation," *Phys. Fluids* **10**, 7.